Surface mixed layer deepening through wind shear alignment in a seasonally stratified shallow sea

Lincoln, Benjamin; Rippeth, Thomas; Simpson, John

Journal of Geophysical Research: Oceans

DOI:
10.1002/2015JC011382

Published: 01/08/2016

Publisher's PDF, also known as Version of record

AGU PUBLICATIONS

JGR

Journal of Geophysical Research: Oceans

RESEARCH ARTICLE

10.1002/2015JC011382

Surface mixed layer deepening through wind shear alignment in a seasonally stratified shallow sea

B. J. Lincoln[1], T. P. Rippeth[1], and J. H. Simpson[1]

[1]School of Ocean Sciences, Bangor University, Bangor, UK

Key Points:
- New observations are presented for surface mixed layer deepening
- The episodes are linked to the alignment of the surface current and wind vector
- The deepening is a result of shear instability and mixing on account of the elevated shear

Correspondence to:
B. J. Lincoln,
ben.lincoln@bangor.ac.uk

Citation:
Lincoln, B. J., T. P. Rippeth, and J. H. Simpson (2016), Surface mixed layer deepening through wind shear alignment in a seasonally stratified shallow sea, *J. Geophys. Res. Oceans*, *121*, doi:10.1002/2015JC011382.

Received 8 OCT 2015
Accepted 22 JUL 2016
Accepted article online 25 JUL 2016

Abstract Inertial oscillations are a ubiquitous feature of the surface ocean. Here we combine new observations with a numerical model to investigate the role of inertial oscillations in driving deepening of the surface mixed layer in a seasonally stratified sea. Observations of temperature and current structure, from a mooring in the Western Irish Sea, reveal episodes of strong currents ($>$0.3 m s^{-1}) lasting several days, resulting in enhanced shear across the thermocline. While the episodes of strong currents are coincident with windy periods, the variance in the shear is not directly related to the wind stress. The shear varies on a subinertial time scale with the formation of shear maxima lasting several hours occurring at the local inertial period of 14.85 h. These shear maxima coincide with the orientation of the surface current being at an angle of approximately 90° to the right of the wind direction. Observations of the water column structure during windy periods reveal deepening of the surface mixed layer in a series of steps which coincide with a period of enhanced shear. During the periods of enhanced shear gradient, Richardson number estimates indicate $Ri^{-1} \geq 4$ at the base of the surface mixed layer, implying the deepening as a result of shear instability. A one-dimensional vertical exchange model successfully reproduces the magnitude and phase of the shear spikes as well as the step-like deepening. The observations and model results therefore identify the role of wind shear alignment as a key entrainment mechanism driving surface mixed layer deepening in a shallow, seasonally stratified sea.

1. Introduction

The surface of the ocean acts as a critical interface within the Earth system, linking the ocean and the atmosphere. The processes which interact to determine surface mixed layer (SML) properties are therefore key determinants of the direction and magnitude of heat and trace gas fluxes across the sea surface [e.g., *Belcher et al*., 2012; *Rippeth et al*., 2014]. Identification and parameterization of the key processes responsible for determining surface mixed layer depth are therefore currently central to the Physical Oceanography agenda. In this paper, we investigate the role of the wind in deepening the surface mixed layer in a seasonally stratified tidally swept shallow sea.

Oscillating currents at, or close to, the local inertial frequency have been widely observed as energetic features in the ocean since they were first reported by *Helland-Hansen and Ekman* [] and appear an almost ubiquitous feature of oceanic motion [e.g., *Pollard*, 1980; *D'Asaro*, 1985; *Jordi and Wang*, 2008; *Hunter et al*., 2007; *Sobarzo et al*., 2007] except where frictional damping is high [*Simpson et al*., 2002]. In consequence, they have been implicated as a major source of mechanical energy which drives diapycnal mixing in the ocean interior [*D'Asaro*, 1985; *Zhang et al*., 2014] and deepens the surface mixed layer of the ocean through driving entrainment [*Pollard et al*., 1972]. While tides account for over 90% of the kinetic energy dissipated within the north-west European shelf sea system, and are the first-order control on water column structure in this region [*Simpson and Hunter*, 1974], a number of studies have suggested that wind initiated inertial oscillations are a key process in driving diapycnal fluxes across the seasonal thermocline [e.g., *Rippeth*, 2005]. Diapcynal mixing and SML deepening provide a key bio geochemical pathway supplying limiting nutrients to the euphoric zone [*Sharples et al*., 2001; *Rippeth et al*., 2009] and thus sustain the primary production once the spring bloom has removed limiting nutrients from the surface layer [*Sharples et al*., 2013].

Sherwin [1987] report episodic inertial oscillations with currents of up to 0.2 m s^{-1} and estimated the rate of production of turbulent kinetic energy through damping of the oscillations concluding that they make

potentially significant contribution to diapycnal mixing in these regions. *MacKinnon and Gregg* [2005] and *Palmer et al*. [2008] report significant levels of baroclinic energy close to the local inertial period for seasonally stratified locations to the east of the U.S. and west of UK, respectively.

Fine-scale velocity and water column structure measurements in a number of seasonally stratified shelf seas have indicated that the gradient Richardson number within the thermocline region is ≈1 [*Chen et al*., 1996; *Van Haren et al*., 1999; *Rippeth*, 2005; *MacKinnon and Gregg*, 2005; *Palmer et al*., 2008; *Rippeth et al*., 2005, 2009], implying that the thermocline is of marginal stability. Phenomena providing addition shear could therefore induce shear instability leading to turbulence and diapycnal mixing across the thermocline. Observations of near-inertial oscillations in seasonally stratified shelf seas have shown the associated currents to be present across the full water column but with a 180° phase shift across the thermocline, indicating that the near-inertial oscillations are a potentially significant source of shear within the seasonally stratified shelf sea thermocline [*Van Haren et al*., 1999; *Knight et al*., 2002; *Rippeth et al*., 2002; *Simpson et al*., 2002].

Rippeth et al. [2009] observed periods of enhanced shear, named "shear spikes" lasting 2–3 h and occurring at intervals separated by approximately one local inertial period. During a shear spike, the observed thermocline averaged value for the rate of dissipation of turbulent kinetic energy (ε) is raised by approximately 3 times above the level observed outside of this period leading to the conclusion that shear instability associated with the enhanced shear leads to the observed elevation of turbulence. Furthermore, they noted that the packets of shear spikes correlated to periods of enhanced wind stress. *Burchard and Rippeth* [2009] develop a simple two-layer model which explained the occurrence of shear spikes as being a result of the alignment of the surface wind vector and the surface current, which is modulated by an inertial oscillation. Using observations of time series of ε, they show that the thermocline averaged value of ε, and hence diapycnal fluxes are raised by a factor of 4 during episodes of shear spiking. The importance of this process in providing key biogeochemical pathways in shelf seas was highlighted by *Williams et al*. [2013] who report significantly enhanced diapycnal nitrate fluxes in response to episodes of shear spikes. Analogous mechanisms have since been implicated in driving enhanced diapcynal mixing beneath sea ice [*Lenn et al*., 2011] and at the base of the oceanic surface mixed layer [*Brannigan et al*., 2013; *Rumyantseva et al*., 2015; *Palter*, 2015].

The aim of this paper is to elucidate the role of near-inertial oscillations in driving surface mixed layer deepening in a seasonally stratified shallow sea with significant tides. In particular, we will examine the role of the alignment of the surface current with the wind in driving shear instability using a combination of observed time series of water column structure and current profiles, from a mooring, together with simulations of water column structure using a one-dimensional numerical model in which vertical exchange is simulated using a turbulence closure scheme.

2. Methodology

2.1. Observations

The area of the study is the Western Irish Sea, a region of significant tidal currents (≈0.3 m s^{-1}) and with a water depth of around 100 m. On account of the water depth and the tidal currents, seasonal stratification is sustained between May and October, with surface to bottom water temperature differences reaching 5–6°C. A mooring was deployed in the zone of seasonal stratification (at 53.47°N 5.38°W, see Figure 1) for a 51 day period between May and July 2009.

The mooring arrangement was designed to resolve processes in the thermocline region with instrumentation focused on the upper half of the water column. Seabird Microcat CTD recorders were located close to the bed and the sea surface measuring time series of temperature, salinity, and pressure. The evolution of stratification was observed using thermistors mounted on the mooring line. The thermistors were set up to record every 60 s and were located in the upper half of the water column, with 20 thermistors, spaced at 2.5 m intervals, between approximately 45 mab and a buoy floating on the sea surface. Every fourth thermistor had a pressure sensor which allowed the location of each thermistor relative to the sea surface to be calculated through linear interpolation. Calibration of thermistors at the beginning and end of deployment required offsets less than 0.05°C and drift observed over the deployment was less than 0.01°C. Analysis of

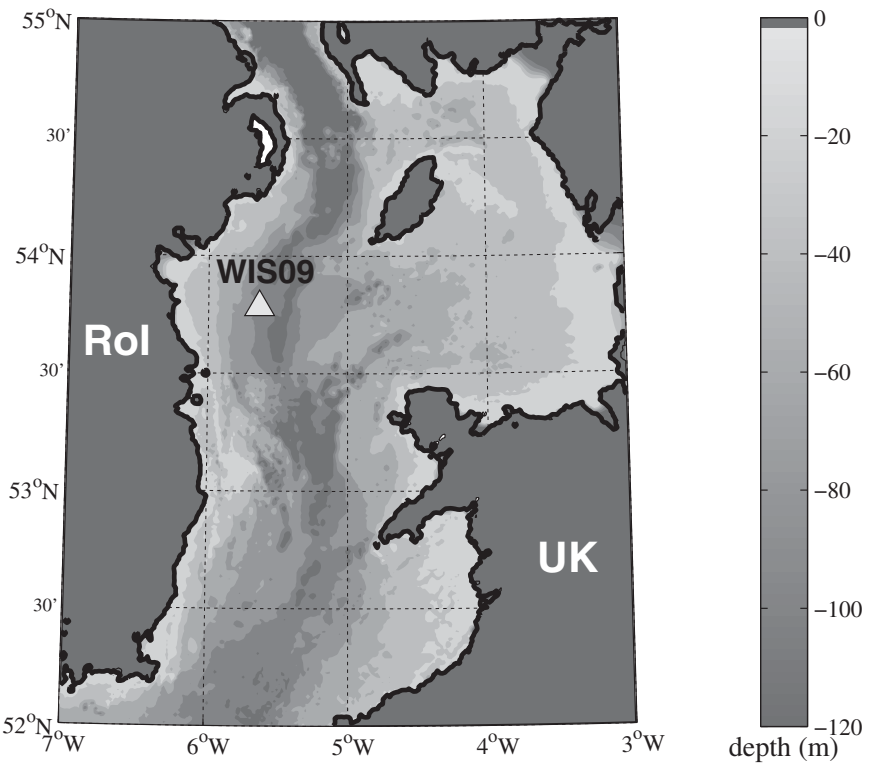

Figure 1. Map showing location of the mooring in the Western Irish Sea, 53°47N 5°38W, 40 km from the coast of the Republic of Ireland.

density profiles taken at the beginning and end of the deployment shows that 85% of the observed vertical variation in density is due to temperature variation.

Vertical profiles of currents were measured by an RDI 600 kHz ADCP mounted in an upward looking mode, on a mid-water float suspended 59 m above the sea bed. This ADCP mooring was located approximately 300 m from the thermistor mooring. The ADCP was set up to measure a current profile every 30 s with a vertical bin size of 0.5 m and sampled the water column between 60 mab and 6 m below the sea surface. Baroclinic velocity profiles were calculated, in order to identify the currents responsible for shear, by removing a depth mean current velocity from each bin. Since the ADCP only sampled the section of the water column above 59 mab, the depth mean velocity is estimated by extrapolating the current estimates from the lower bin of the ADCP down to a depth of 15 mab. This extrapolation was validated against a hind-cast made using a tidal fit to full water column velocities measured from a bed mounted ADCP deployed at this location later in same year (not presented).

The bulk shear, S_b, is calculated using the velocity time series data collected by the mid-water column ADCP, which had a 5 min temporal and 0.5 m vertical resolution using the equation:

$$S_b^2 = \left(\frac{u_s - u_b}{h_{diff}}\right)^2 + \left(\frac{v_s - v_b}{h_{diff}}\right)^2 \quad (1)$$

where v_s, u_s, v_b, and u_b are the northerly and easterly velocity components above and below the thermocline, averaged over the ranges, s = 83–87 mab, b = 59–64 mab. h_{diff} = 23 m is the distance between the mean height of the two layers. Since the low-frequency shear is of interest, the layer velocities were filtered to give an hourly running mean.

Since the anemometer on the mooring Met Package failed a time series of local wind was extracted from the UK Meteorological office mesoscale model. The model integrates land and ocean-based observations to model the wind field across the British Isles providing 3 hourly wind speed and direction at a horizontal resolution of 11 min.

2.2. One-Dimensional Model

To investigate further the evolution of inertial oscillations and their impact on the surface mixed layer, a one-dimensional vertical exchange model was used to simulate the velocity profile and vertical density structure for the mooring location. The model [*Simpson and Sharples*, 2012] solves the linearized form of the horizontal momentum equations (1)

$$\frac{\partial u}{\partial t} = -\frac{1}{\rho}\left(\frac{\partial p}{\partial x} + \frac{\partial \tau_x}{\partial x}\right) + fv + \frac{\partial}{\partial z}\left(N_z \frac{\partial u}{\partial z}\right) \tag{2}$$

$$\frac{\partial v}{\partial t} = -\frac{1}{\rho}\left(\frac{\partial p}{\partial y} + \frac{\partial \tau_y}{\partial y}\right) - fu + \frac{\partial}{\partial z}\left(N_z \frac{\partial v}{\partial z}\right) \tag{3}$$

where the easterly and northerly velocity components, u and v, are calculated at each depth z. Tidal motions are forced by a surface pressure gradient, which was calculated from a surface slope where $\left(\frac{\partial p}{\partial x}, \frac{\partial p}{\partial x}\right) = -\rho g\left(\frac{\partial \eta}{\partial x}, \frac{\partial \eta}{\partial y}\right)$. Surface slopes were calculated from tidal fits to the observed current data for the dominant M2 and S2 tidal components. Stress components τ_x and τ_y are calculated at the bed using a standard quadratic drag law. The surface stress was also calculated using a standard quadratic drag law and drag coefficient calculated according to *Yelland and Taylor* [1996] from 3 hourly wind estimates from the UK Meteorological office mesoscale model output for this location.

Since the aim of the modeling exercise is to examine the role of the shear spike mechanism in surface mixed layer development no exchange of heat across the sea surface was permitted within the model. Vertical transfer of momentum and density is described by an eddy viscosity N_z and eddy diffusivity, which are related to the shear and stratification by a Mellor-Yamada 2.2 turbulence closure scheme with turbulence allowed to diffuse at the same rate as momentum following *Simpson et al*. [1996] and using Richardson number-dependent stability functions based on a local equilibrium [*Galperin et al*., 1988].

3. Results

3.1. Hydrology and Meteorology

The deployment period covered the onset and development of stratification, with the sea surface temperature increasing from 10°C to 16°C, while the deep water (below 50 mab) remained at a temperature below 11°C. The evolution of the water column structure over the 51 days of the mooring deployment, together with the surface wind stress, tidal range, and the bulk shear across the thermocline, are shown in Figure 2. Periods of strong surface warming, days 150–157 and 175–185, are separated by periods of enhanced wind stress associated with the passage of atmospheric low-pressure systems. During the period of the observations, these systems pass through approximately every fortnight and last several days. During the passage of the low-pressure systems, the surface mixed layer is observed to cool and deepen. The largest shears are also observed across the thermocline at these times, with shear taking the form of significant enhancements (spikes) lasting several hours which are separated from one another by approximately one local inertial period (14.85 h). Peak barotropic tidal currents of 0.2–0.4 m s^{-1} are observed at spring and neaps, respectively. Baroclinic tidal currents are observed during spring tides with peak magnitudes of 0.1 m s^{-1}. During neap tides, the baroclinic tidal currents were found to be several centimeters a second, an order of magnitude lower than peak inertial current velocities.

Here we focus on one period of significant shear enhancement and surface mixed layer deepening coincident with a period of high wind stress and relatively small tides on days 180–187 (identified Figure 2b).

3.2. Shear Observations

The evolution of the surface mixed layer together with the bulk shear and wind stress for the identified period of interest are shown in Figure 3. The water column was strongly stratified throughout, with a sea bed to sea surface temperature difference of 5°C largely concentrated across a thermocline which is about 20 m thick. At the start of this period (day 182), the thermocline is diffuse occupying the upper 30 m of the water column below a surface mixed layer of about 5 m. The wind stress is low ($\tau_s < 0.03$ Pa) as is the bulk shear, $S_b^2 < 5 \times 10^{-5}$ m^2 s^{-2} (Figure 3c). On day 183, an atmospheric low-pressure system arrived in the area, with a consequent 20 mB drop in atmospheric pressure accompanied by a rapid increase in wind stress to

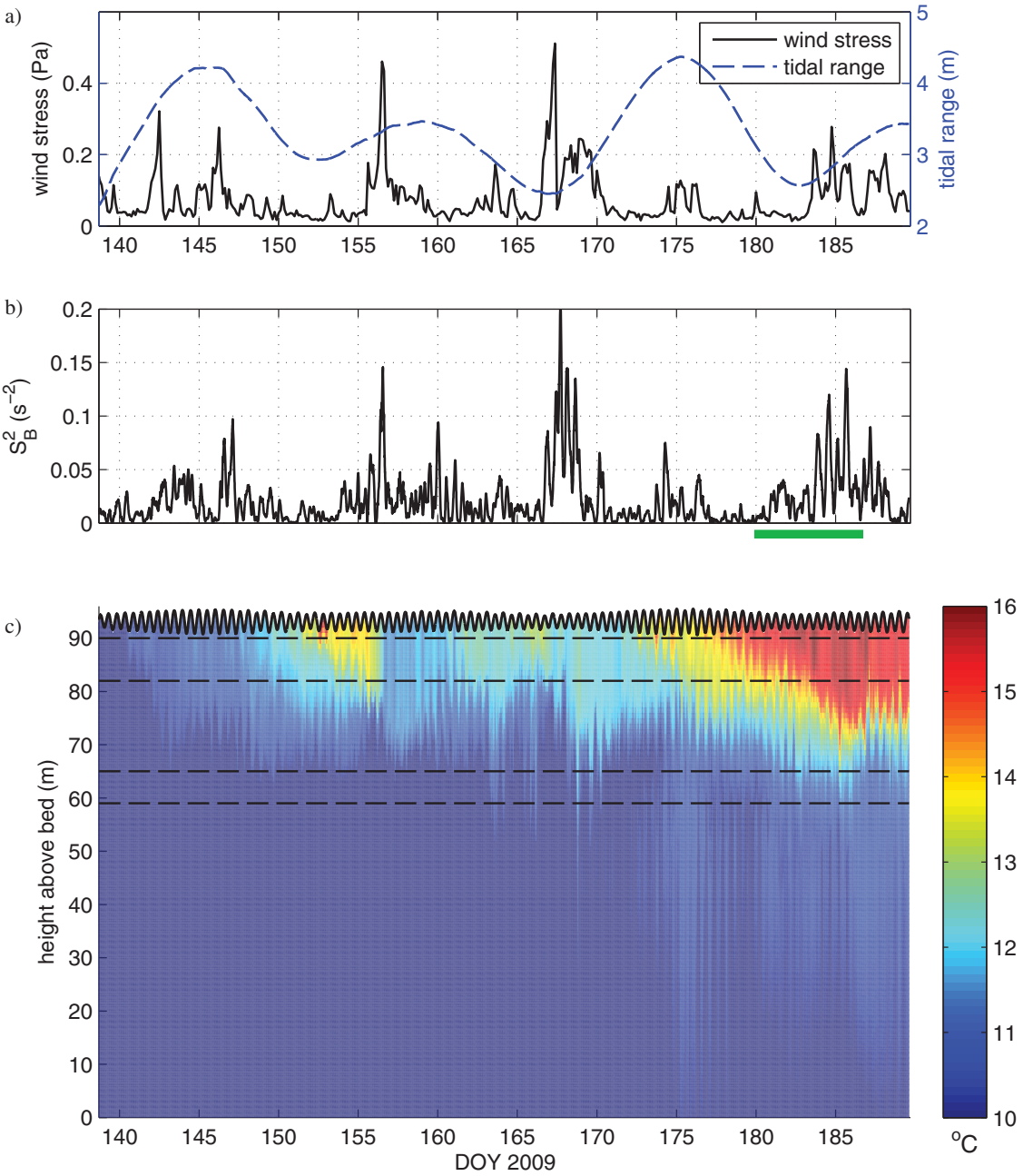

Figure 2. Mooring data showing bulk shear over the entire mooring deployment. (a) Wind stress from met office reanalysis (solid line) and tidal amplitude from bed mounted pressure recorder (dashed line). (b) Magnitude of bulk shear squared, S2b, calculated from mean velocity above (80–88 mab) and below the thermocline (60–65 mab) using a 2 h moving average. (c) Vertical temperature structure from moored thermistors, dashed lines show regions used to calculate S2b.

$\tau_s > 0.2$ Pa. The wind stress remained high for approximately 3 days (Figure 3a) with the wind blowing toward the northeast (i.e., a south-westerly in meteorological terms). During the episode of elevated wind stress, a series of periods of enhanced shear, with peak magnitudes of $S_b^2 > 2 \times 10^{-4}$ m^2 s^{-2}, are observed and have been labeled 1–5 for reference. Between these periods of enhanced shear, S_b falls close to zero. The separation between the periods of enhanced shear is close to the local inertial period. The periods of enhanced S_b do not correlate with periods of high τ_s. In fact the largest value of τ_s is actually observed to occur at a time when there was virtually no bulk shear (day 184.8).

During the periods of enhanced shear, strong baroclinic currents (Figure 3b) are observed in the surface mixed layer $\sqrt{(u_s^2 + v_s^2)} = 0.3$m s^{-1}, with weaker baroclinic currents $\sqrt{(u_s^2 + v_s^2)} = 0.05$ m s^{-1} below the

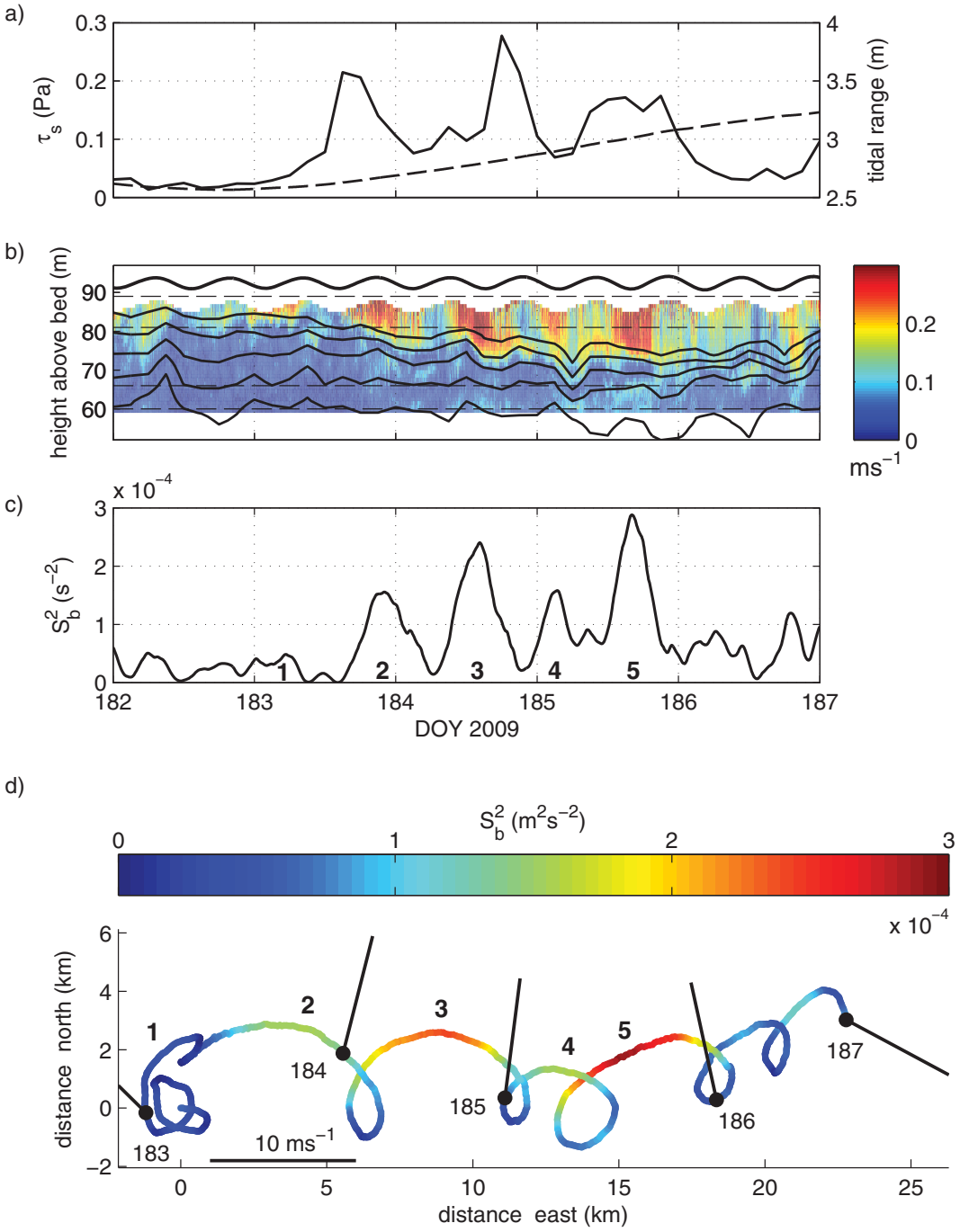

Figure 3. Mooring observations showing a series of inertial oscillations in the surface layer accompanied by spikes in the bulk shear. (a) Wind stress from Met Office 3 h reanalysis wind speed model (solid line) and range of tidal elevation (dashed line). (b) Magnitude of baroclinic velocity, √(u2+v2), with 1°C temperature contours overlaid (10–13°C). (c) Magnitude of bulk shear squared, S_b2, calculated from layer mean velocity from region above and below the thermocline, as indicated in Figure 3b. (d) Progressive vector plot of the surface layer baroclinic motion with wind vector. The color of the plot indicates the magnitude of shear, with peaks 1–5 occurring when surface layer velocity is 90° to the right of the wind.

thermocline which were 180° out of phase with those in the SML. The phase shift between the surface mixed layer and lower layer currents is consistent with previously reported observations of inertial oscillations in shelf seas [e.g., *Van Haren et al.*, 1999; *Knight et al.*, 2002; *Rippeth et al.*, 2002; *Simpson et al.*, 2002]. Within the interior of the thermocline, baroclinic current velocities remained low. The SML currents are observed to be uniform with depth suggesting that the surface mixed layer is acting as a slab moving over

a quiescent thermocline. Over this period, the surface mixed layer depth increases from 5 to over 20 m, while the thermocline thickness decreases (Figure 3b). The SML is observed to deepen during each shear spike. During this period the sea surface temperature was observed to drop by 0.5°C. This fall is smaller than expected for the observed entrainment of cooler thermocline water into the SML during the deepening events implying some other process is acting to raise the temperature of the SML at the same time. While advective effects cannot be ruled out, an additional surface heat input of 200 W m^{-2} is sufficient to account for the difference between the observed temperature change and that implied by the entrainment of cooler thermocline water into the SML as a result of the deepening. This is a reasonable value for the net heat flux, at this location, at this time of the year and similar to that observed over days prior to the deepening event.

Baroclinic currents below the SML are significantly smaller than those within it, indicating that the shear across the thermocline is primarily due to the SML currents. The relationship between the wind, SML currents, and shear is visualized using a progressive vector plot (Figure 3d) where the color of the path indicates the magnitude of S_b^2. The path of the SML describes a series of inertial oscillations with a diameter several km superimposed over an easterly drift of 25 km over 5 days. Weak winds blowing toward the west at the start of the period coincide with small currents, weak shear and small oscillations. As the wind speed increases on day 183, the series of large inertial oscillations are formed corresponding to the numbered spikes. The noncircularity of these inertial motions is due to the continued action of the wind throughout, which blows to the north, accelerating the SML during the northerly half of the oscillations and retarding it in the southerly half. The color of the path shows that subsequent spikes in shear, numbered 2–5, occur when SML currents are greatest, and directed toward the East and at right angles to the wind direction.

The shear may be considered as a series of inertial oscillations superimposed over an Ekman current which occurs 90° to the right of the wind. Decomposition of the surface currents into inertial and sub inertial components (not plotted) reveals inertial oscillations which are circular with a magnitude of 0.06–0.18 m s^{-1} accompanied by a subinertial flow of 0.06 m s^{-1} to the east. In order to further investigate this interaction between the wind forcing and SML currents, we employ an analytical two layered model.

3.3. Shear Production Model

A key observation is that the peak in shear actually occurs sometime after the alignment of the wind stress with the surface current. The magnitude of the shear across the thermocline is shown, together with the angle between the direction of the wind and shear vectors, in Figure 4. Figure 4c shows that in all four cases the peak shear occurs when the current vector is orientated at approximately 90° to the right of the wind vector, showing that the peak shear occurs at approximately one quarter of a local inertial period (i.e., 3 h 45 min for this location) after the alignment of the wind and shear vectors. The development of periods of enhanced shear together with the delay in the maximum shear of approximately one fourth of a local inertial period after the alignment of the surface current vector with the surface wind stress are entirely consistent with the model for the development of "shear spikes," in the shelf sea seasonal thermocline, of *Burchard and Rippeth* [2009, hereafter BR09].

BR09 used a two-layer model to describe the impact of the wind and tidal stresses on the shear within the thermocline region in a stratified shelf sea (equation (2)). The model predicts the rate of production of shear, $P(S^2)$, as the dot product of the bulk shear vector, $\vec{S}$, and wind stress vector, $\vec{\tau}_s$, on the sea surface, and the bed stress vector, $\vec{\tau}_b$. The maximum rate of production of shear corresponds to the time when the bulk shear vector, wind stress vector and bed stress vector are aligned.

$$P(S^2) = \frac{4}{h}\vec{S}.\left(\frac{\vec{\tau}_s}{h_s} + \frac{\vec{\tau}_b}{h_b}\right) \tag{4}$$

The shear will continue to grow while $P(S^2) > 0$, with the spike corresponding to $P(S^2) = 0$.

Using the reanalysis winds and the ADCP current profiles, time series of $\vec{S}$, $\vec{\tau}_s$, and $\vec{\tau}_b$, are generated using quadratic drag laws using coefficients of $C_d = 0.0015$ for $\vec{\tau}_b$ and C_d calculated according to Yelland and Taylor for $\vec{\tau}_s$. $P(S^2)$ is then calculated using equation (4), taking values of $h_s = 10$ m and $h_b = 75$ m are shown in Figure 4. The excellent agreement between the observed time evolution of the bulk shear vector, $\delta_t S^2$ plotted as dots in Figure 4b, and that predicted by the model, $P(S^2)$, plotted as a line, indicates that the model contains all of the necessary physics to explain to the first order the observed development of the periods of enhanced shear. The BR09 model was originally used to explain the development of shear spikes in the

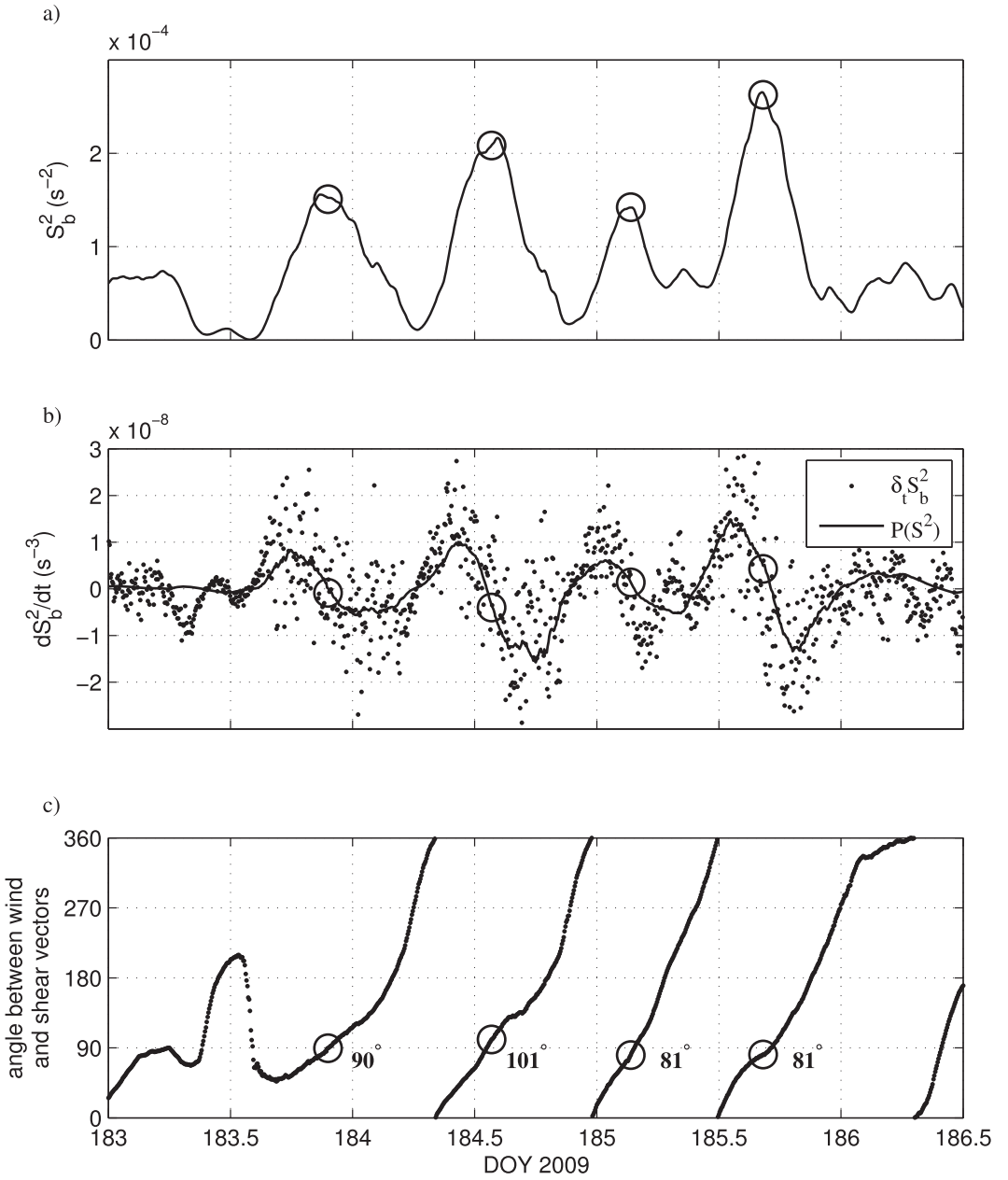

Figure 4. A comparison of the observed rate of change of shear with that predicted by Burchard-Ripperth model. (a) Magnitude of bulk shear squared, Sb2. (b) Time derivative of bulk shear squared, dSb2/dt and production of bulk shear squared P(Sb2) as predicted by Burchard Ripperth model (equation (4)). (c) The clockwise angle from the shear vector to the wind vector. The circles indicate the peaks of the shear spikes and occur when: P(Sb2) = 0 and ∼ts is ∼90° clockwise from $\vec{S}$.

shelf sea seasonal thermocline during the autumn, when the surface and bottom mixed layers are of similar thickness. In this case the stratification exhibits a 3 layered structure with a significant thermocline thickness, while the surface layer thickness is small but growing with $h_s = 5$–15 m and a bottom layer thickness of $h_b \sim 70$ m. The order of magnitude difference in the denominators, h_s and h_b, in equation (3) implies that the production of shear is dominated by the wind stress term with a negligible contribution from the bed stress term. Furthermore, the period of interest happens to coincide with neaps tides and so the bed stress due to the tidal currents is low.

The circles plotted in Figure 4 indicate the peak values in S_b^2 and that they coincide with the instant when the sign of the production term switches from positive to negative. Figure 4c shows the difference in angle

between the wind and the bulk shear vector. The positions of the circles plotted show that each peak occurred when the wind direction was at an angle of ≈90° to the right of the bulk shear vector. At this time the wind stress starts to oppose the surface current (i.e., $P(S^2) < 0$). This effect is evident in the surface layer motion (Figure 3) and is predicted by the BR09 model in which the effects of the bed stress are neglected, i.e.,

$$P(S^2) = \frac{4}{h}\vec{S}.\frac{\vec{\tau}_s}{h_s} \tag{5}$$

Solutions to equation (3) which satisfy $P(S^2) = 0$ occur when the vectors $\vec{S}$ and $\vec{\tau}$ are perpendicular to each other. If the wind direction remains constant, then the shear spikes will be separated by a period which corresponds to the local inertial period. However, if the wind veers the period of separation will decrease as observed between shear spikes 4 and 5 (Figure 3).

3.4. Mixed Layer Deepening and Shear Instabilities

The observations presented above show that the surface mixed layer deepening occurs in steps which coincide with the occurrence of the spikes in shear. To investigate the potential of the shear to destabilize the upper part of the thermocline, and so trigger shear instability and mixing, a time series of the gradient Richardson number, $Ri = N^2/S^2$ is calculated using the fine-scale velocity and temperature measurements. The gradient Richardson number quantifies the balance of destabilizing stresses due to sheared flow against the stabilizing buoyancy forces arising from stratification. When the shear stresses become sufficient to overcome buoyancy forces ($Ri \leq 0.25$), the formation of billows occurs and turbulence develops. Hourly averaged vertical profiles of shear squared, S^2 are interpolated onto a common 2.5 m vertical grid determined by the heights of the moored thermistors. Hourly averaged vertical density profiles were then calculated using the temperature profiles, from the moored thermistors, assuming that the observed change in density is due to the change in temperature. A time series of vertical profiles of buoyancy frequency, $N^2 = \frac{g}{\rho_0}\frac{\Delta\rho(z)}{d\Delta z}$, was then calculated from the density profiles. The time series showing the evolution of S^2, N^2, together with the estimated inverse Richardson number, Ri^{-1}, for the period of interest is given in Figure 5.

In the early part of the time series, the diffuse pycnocline is evident in the low buoyancy frequency estimates, $N^2 < 4 \times 10^{-4}$ m^2 s^{-2}, which are observed across a broad depth range of 60–90 mab. Shear is modest, $S^2 \sim 6 \times 10^{-4}$ m^2 s^{-2} and confined to the upper 10 m, limiting the lower layer stability, i.e., $Ri^{-1} > 1$, to the shallow SML. The high shear associated with the spikes is confined to 5–10 m thick regions (Figure 5b), where $S^2 > 1 \times 10^{-3}$ m^2 s^{-2}. The region of enhanced shear associated with each successive spike occurs lower in the water column. Each of the first three spikes (1–3) coincide with a significant deepening of the surface mixed layer (in steps of ∼5 m, Figure 5c), although there is a slight reduction in the depth of the SML as the shear declines following each spike. The first three spikes generate sufficient shear to reduce the Richardson number below the critical threshold at which shear instability, and thus mixing, may be initiated, e.g., $Ri^{-1} \geq 4$, for periods of several hours. Shear spikes 4 and 5 were less effective at lowering the Richardson number despite the largest observed shear being associated with spike 4. As the mixed layer deepened, the magnitude of the buoyancy frequency increased, $N^2 \sim 8 \times 10^{-4}$ m^2 s^{-2}, and in consequence the enhanced shear associated with shear spikes 4 and 5 was less effective at inducing shear instability.

The observations presented demonstrate that the shear spikes act as an intermittent form of boundary mixing, generating strong shear at the base of the surface mixed layer which erodes the top of the thermocline resulting in surface mixed layer deepening. The nature of the process results in the SML deepening taking place through a number of discrete entrainment events separated by a time period, which corresponds to the local inertial period providing the wind direction remains constant.

Strong observational evidence has been presented to support the role of shear spikes, resulting from the alignment of the surface current with the surface wind stress, in driving the deepening of the surface mixed layer. However, using the observations available it is not possible to separate out the potential additional contribution of the background internal wavefield, horizontal advection or wave-driven mixing effects, e.g., Langmuir circulation, to the surface mixed layer development during the observed deepening. In order to test the hypothesis that the SML deepening is a result of shear spikes in isolation a one-dimensional vertical exchange model is used.

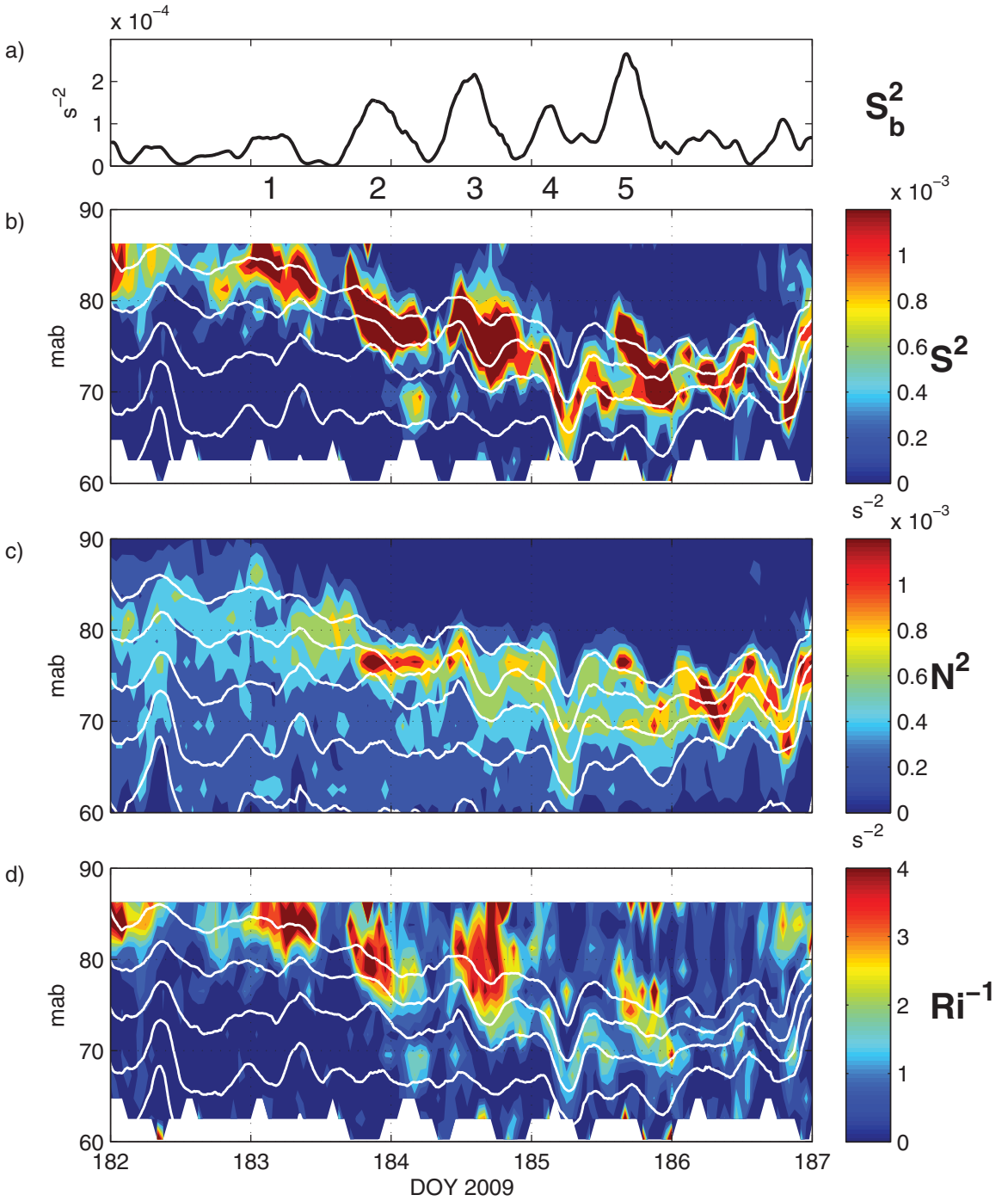

Figure 5. Shear, stratification, and Richardson number from the moorings during the shear spikes. (a) Magnitude of the bulk shear squared, Sb2. (b) The vertical structure of S2. (c) The vertical structure of N2. (d) The vertical structure of Ri^{-1}. The shear spikes reduce the Richardson number to ~0.25 ($Ri^{-1} \sim 4$) and erode the thermocline deepening the SML while the magnitude of N2 increases. The white contours indicate the height of the 11°C–15°C isotherms.

3.5. Turbulence Closure Model Predictions

The one-dimensional vertically resolving turbulence closure-based vertical exchange model is forced using the observed tides and winds for the period covering the observational period of interest. While momentum transfer across the sea surface is permitted, heat exchange is not. The model is initialized by setting the vertical density structure to that observed at the moorings at the start of the period of interest. The model is then run for a 10 day spanning the period of the observed shear spikes.

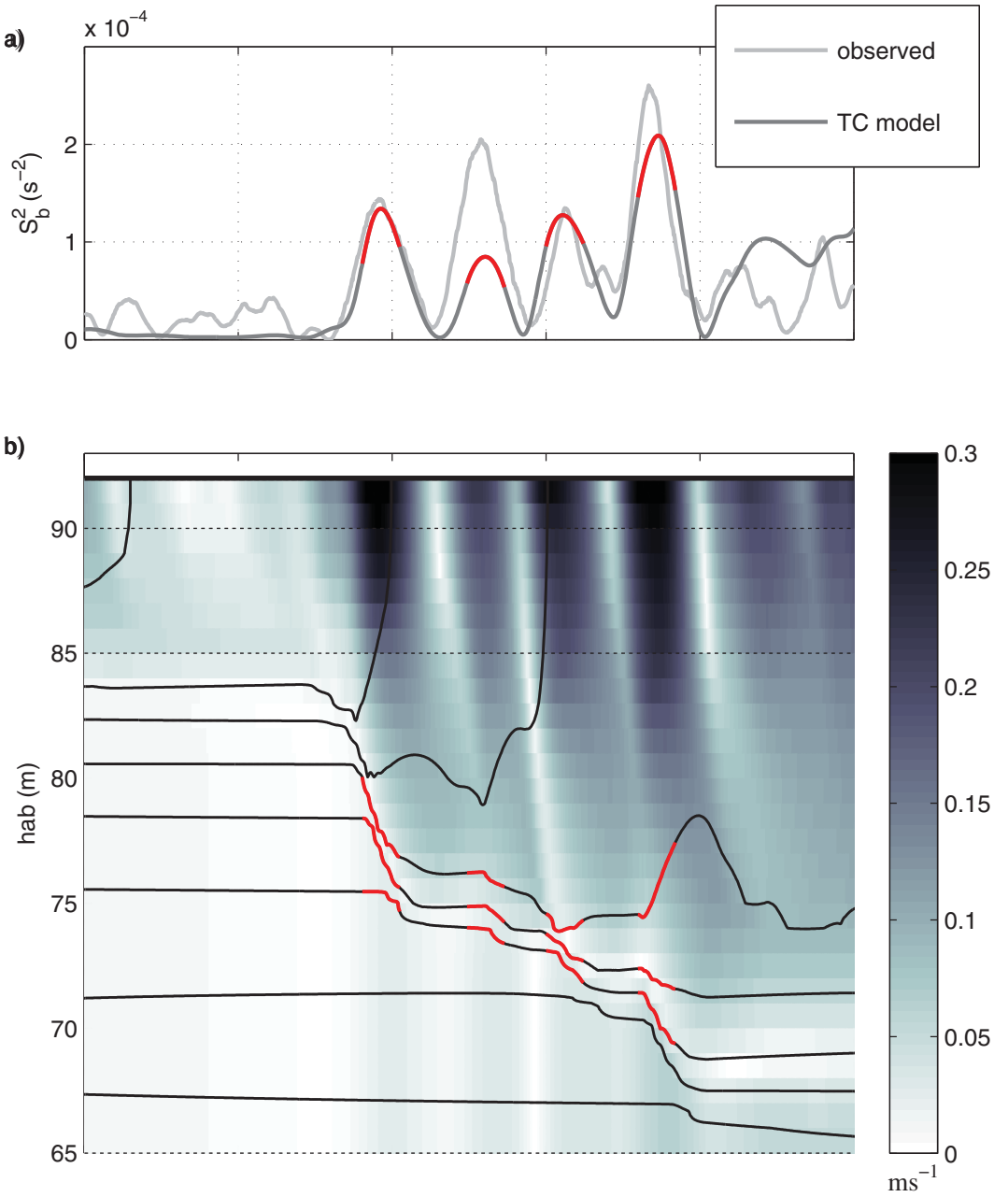

Figure 6. Output from a 1-D TC model showing reproduction of shear spikes and periodic deepening coincident with peak shear. (a) Magnitude of bulk shear squared, S_b^2, from model (black line) and observations (grey line). (b) Total baroclinic velocity magnitude with density isopycnal contours overlaid (1025–1026 kg m^{-3} every 0.25 kg m^{-3}).

The one-dimensional model is able to reproduce many of the observed features of the deepening events (Figure 6). In particular, the large inertial currents in the surface layer are predicted together with the interaction with the wind which results in the generation of the spikes in the bulk shear. The predicted shear spikes are of similar magnitude (Figure 6a) and phasing to those observed. Furthermore, the model predicts the observed deepening of the surface mixed layer in response to the shear spikes. Figure 6b shows the deepening of isotherms coincident with the peak shear enhancement during the spikes forming a series of steps as the SML deepens. Upper isotherms are seen to shoal as cooler water is entrained. This result confirms that the physics contained in this 1-D model is sufficient to describe the shear spike generation and step wise deepening in this situation.

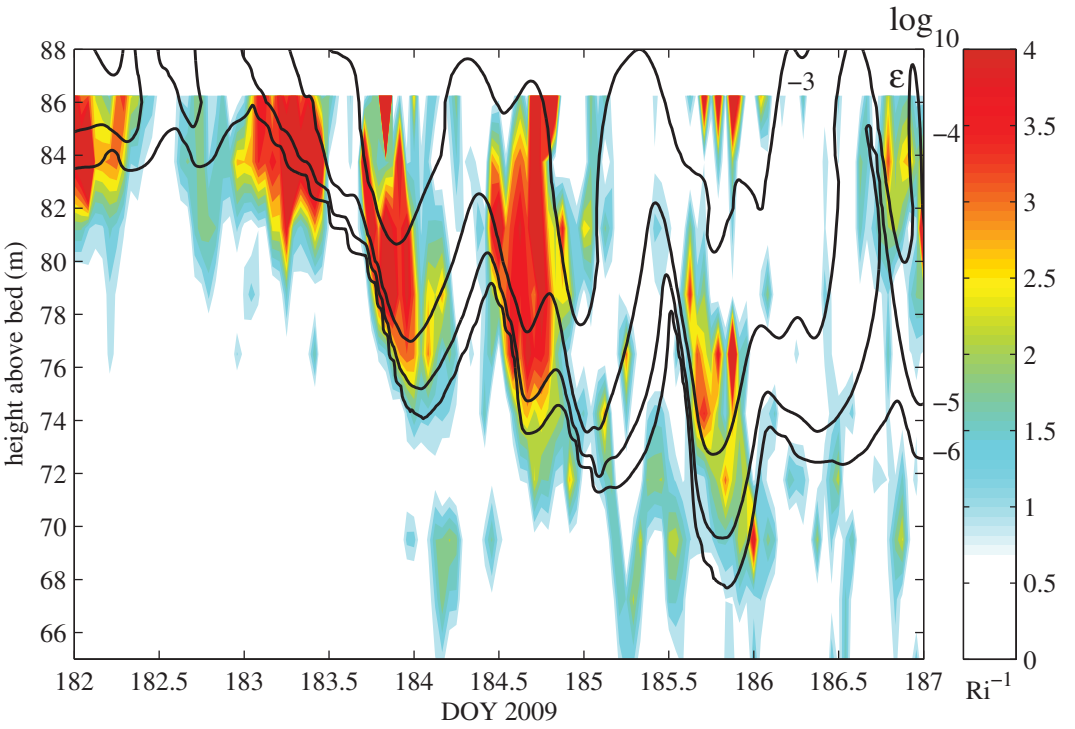

Figure 7. Turbulent kinetic energy dissipation rate ($\log_{10}$ W m^{-3}) predicted by 1-D TC model overlying color plot of the inverse Richardson number calculated from the moored observations. Low stability conditions observed in the mooring measurements are predicted to be regions of enhanced mixing propagating down from the surface.

The maximum predicted TKE dissipation rate, ε, occurs during the spikes and close to the surface, with ε decreasing at the thermocline. Four observed spikes are predicted by the model which also shows corresponding instabilities and elevated ε extending down from the surface as the SML deepens (Figure 7). However, while the observations appear to show the surface mixed layer moving as a slab, with uniform velocity over depth, the model predicts a phase lag in the maximum current speed which increases with depth over the surface mixed layer which may indicate key physical processes are not present in the model.

4. Discussion

Here we have combined observations with the shear spike model of *Burchard and Rippeth* [2009] and a one-dimensional vertically resolving numerical model to demonstrate, for the first time, the role of shear instability, in damping inertial oscillations and driving mixing, facilitated by periods of enhanced shear resulting from wind shear alignment, in driving surface mixed layer deepening in a seasonally stratified, tidally swept shallow sea. While previous measurements have focused on the later stages of an inertial oscillations life, the new measurements presented here show the evolution of the surface mixed layer through the initiation of the inertial oscillation. A key consequence of this study is therefore to highlight the major role played by the wind in driving vertical mixing in seasonally stratified shelf seas, despite the tide dominating the local kinetic energy budget in these regimes. As inertial oscillations are a transient in the development of an Ekman current these results coupled with the BR09 model also suggest that the development Ekman currents will be influenced by the ratio of SML and bottom boundary layer depths in tidally swept shelf seas. The one-dimensional model reproduced the essential dynamics of the wind-shear interaction including the SML deepening. However, there is one significant discrepancy between the modeled and observed surface layer currents: the phase of the SML current is predicted to lag with depth. This lag was not present in the observed velocities. This discrepancy may be a result of neglect of physical processes such as the influence of surface waves and Langmuir circulation within the turbulence closure model.

The surface mixed layer deepening events presented are a consequence of the windy conditions which accompany the passage of low-pressure systems as they cross the Irish Sea. During the 50 day time series

collected in the summer of 2009 there were four such events, each of which resulted in inertial currents, spikes in the bulk shear and significant surface mixed layer deepening. The occurrence of such events will vary on monthly and interannual time scales. As summer weather conditions over this region are largely determined by large-scale atmospheric circulation patterns over the North Atlantic [*Sutton and Dong*, 2012] one would expect variability in the wind contribution to mixing to be influenced by large-scale climatic conditions.

Previous work has highlighted the key role of the shear spike mechanism in supplying limiting nutrients to the euphotic zone and therefore supporting primary productivity within seasonally stratified shelf seas [*Williams et al*., 2013]. The wind shear alignment and SML deepening mechanism reported here may therefore provide a causal link between the larger-scale climate (NAO) variability and the level of primary production in seasonally stratified shelf seas, and so contribute to the reported correlations between climatic variability and marine ecosystem dynamics in shelf seas [e.g., *Attrill and Power*, 2002].

Acknowledgments
We thank the crew of the RV Prince Madog and the Bangor University technicians, in particular Ben Powell and Ray Wilton, for their help and expertise in constructing and deploying the moorings. Funding for the data collection and analysis was provided by the UK Natural Environmental research council through grant NE/F002858/1. B.J.L. was supported by an NERC PhD studentship. The data used in this paper are available on request from the British Oceanographic Data Centre (bodc.ac.uk).

References

Attrill, M. J., and M. Power (2002), Climatic influence on a marine fish assemblage, *Nature*, *417*, 275–278.
Belcher, S. E., et al. (2012), A global perspective on Langmuir turbulence in the ocean surface boundary layer, *Geophys. Res. Lett.*, *39*, L18605, doi:10.1029/2012GL052932.
Brannigan, L., Y. D. Lenn, T. P. Rippeth, E. McDonagh, T. K. Chereskin, and J. Sprintall (2013), Shear at the base of the oceanic mixed layer generated by wind shear alignment, *J. Phys. Oceanogr.*, *43*, 1798–1810.
Burchard, H., and T. P. Rippeth (2009), Generation of bulk shear spikes in shallow stratified tidal seas, *J. Phys. Oceanogr.*, *39*(4), 969–985.
Chen, C., R. O. Reid, and W. D. Nowlin Jr. (1996), Near-inertial oscillations over the Texas-Louisiana shelf, *J. Geophys. Res.*, *101*, 3509–3524.
D'Asaro, E. (1985), The energy flux from the wind to near-inertial motions in the surface mixed layer, *J. Phys. Oceanogr.*, *14*, 1043–1059.
Galperin, B., L. H. Kantha, S. Hassid, and A. Rosati (1988), A quasi-equilibrium turbulent energy model for geophysical flows, *J. Atmos. Sci.*, *45*(1988), 55–62.
Ekman, V.W. and Helland-Hansen, B., Measurements of ocean currents (experiments in the North Atlantic), *Kgl. Fysiogr. Sallsk. Lund*, *1*(1), 7pp.
Hunter, E., R. Chant, L. Bowers, S. Glenn, and J. Kohut (2007), Spatial and temporal variability of diurnal wind forcing in the coastal ocean, *Geophys. Res. Lett.*, *34*, L03607, doi:10.1029/2006GL028945.
Jordi, A., and D.-P. Wang (2008), Near-inertial motions in and around the Palamos submarine canyon (NW Mediterranean) generated by a severe storm, *Cont. Shelf Res.*, *28*(17), 2523–2534.
Knight, P. J., M. J. Howarth, and T. P. Rippeth (2002), Inertial oscillations in the northern North Sea, *J. Sea Res.*, *47*, 269–284.
Lenn, Y.-D., T. P. Rippeth, C. P. Old, S. Bacon, I. Polyakov, V. Ivanov, and J. Hölemann (2011), Intermittent intense turbulent mixing under ice in the Laptev Sea Continental Shelf, *J. Phys. Oceanogr.*, *41*(3), 531–547.
MacKinnon, J. A., and M. C. Gregg (2005), Near-inertial waves on the New England Shelf: The role of evolving stratification, turbulent dissipation, and bottom drag, *J. Phys. Oceanogr.*, *35*, 2408–2424.
Palmer, M. R., T. P. Rippeth, and J. H. Simpson (2008), An investigation of internal mixing in a seasonally stratified shelf sea, *J. Geophys. Res.*, *113*, C12005, doi:10.1029/2007JC004531.
Palter, J. (2015), Storms bring ocean nutrients to light, *Nature*, *525*, 460–461.
Pollard, R. T. (1980), Properties of near-surface inertial oscillations, *J. Phys. Oceanogr.*, *10*, 385–398.
Pollard, R. T., P. B. Rhines, and R. O. R. Y. Thompson (1972), The deepening of the wind-Mixed layer, *Geophys. Fluid Dyn.*, *4*(1), 381–404.
Rippeth, T. P. (2005), Mixing in seasonally stratified shelf seas: A shifting paradigm, *Philos. Trans. R. Soc. A.*, *363*(1837), 2837–2854.
Rippeth, T. P., J. H. Simpson, R. J. Player, and M. Garcia (2002), Current oscillations in the diurnal-inertial band on the Catalonian shelf in spring, *Cont. Shelf Res.*, *22*(2), 247–265.
Rippeth, T. P., M. R. Palmer, J. H. Simpson, N. R. Fisher, and J. Sharples (2005), Thermocline mixing in summer stratified continental shelf seas, *Geophys. Res. Lett.*, *32*, L05602, doi:10.1029/2004GL022104.
Rippeth, T. P., P. Wiles, M. R. Palmer, J. Sharples, and J. Tweddle (2009), The diapcynal nutrient flux and shear-induced diapcynal mixing in the seasonally stratified western Irish Sea, *Cont. Shelf Res.*, *29*(13), 1580–1587.
Rippeth, T. P., B. J. Lincoln, H. A. Kennedy, M. R. Palmer, J. Sharples, and C. A. J. Williams (2014), Impact of vertical mixing on sea surface pCO2 in temperate seasonally stratified shelf seas, *J. Geophys. Res. Oceans*, *119*, 3868–3882, doi:10.1002/2014JC010089.
Rumyantseva, A., N. Lucas, T. Rippeth, A. Martin, S. C. Painter, T. J. Boyd, and S. Henson (2015), Ocean nutrient pathways associated with the passage of a storm, *Global Biogeochem. Cycles*, *29*, 1179–1189, doi:10.1002/2015GB005097.
Sharples, J., C. M. Moore, and E. R. Abraham (2001), Internal tide dissipation, mixing, and vertical nitrate flux at the shelf edge of NE New Zealand. *J. Geophys. Res.*, *106*, 14,069–14,081.
Sharples, J., B. E. Scott, and M. E. Inall (2013), From physics to fishing over a shelf sea bank, *Prog. Oceanogr.*, *117*, 1–8, doi:10.1016/j.pocean.2013.06.015.
Sherwin, T. (1987), Inertial oscillations in the Irish Sea, *Cont. Shelf Res.*, *7*(2), 191–211.
Simpson, J. H., and J. Hunter (1974), Fronts in the Irish Sea, *Nature*, *250*, 404–406.
Simpson, J. H., and J. Sharples (2012), *An Introduction to the Physical and Biological Oceanography of Shelf Seas*, 424 pp., Cambridge Univ. Press., Cambridge, U. K.
Simpson, J. H., W. Crawford, T. P. Rippeth, A. R. Campbell, and J. V. S. Cheok (1996), The vertical structure of turbulent dissipation in shelf seas, *J. Phys. Oceanogr.*, *26*, 1579–1590.
Simpson, J. H., P. Hyder, T. P. Rippeth, and I. M. Lucas (2002), Forced Oscillations near the critical latitude for diurnal-inertial resonance, *J. Phys. Oceanogr.*, *32*, 177–187.
Sobarzo, M., R. K. Shearman, and S. Lentz (2007), Near-inertial motions over the continental shelf off Concepcion, central Chile, *Prog. Oceanogr.*, *75*(3), 348–362.
Sutton, R. T., and B.-W. Dong (2012), Atlantic Ocean influence on a shift in European climate in the 1990s, *Nat. Geosci.*, *5*, 788–792.

Van Haren, H., L. Maas, J. T. F. Zimmerman, H. Ridderinkhof, and H. Malschaert (1999), Strong inertial currents and marginal internal wave stability in the central North Sea, *Geophys. Res. Lett.*, *26*, 2993–2996.

Williams, C., J. Sharples, C. Mahaffey, and T. Rippeth (2013), Wind-driven nutrient pulses to the subsurface chlorophyll maximum in seasonally stratified shelf seas, *Geophys. Res. Lett.*, *40*, 5467–5472, doi:10.1002/2013GL058171.

Yelland, M., and P. Taylor (1996), Wind stress measurements from the open ocean, *J. Phys. Oceanogr.*, *26*(4), 541–558.

Zhang, S., L. Xie, Y. Hou, H. Zhao, Y. Qi, and X. Yi (2014), Tropical storm-induced turbulent mixing and chlorophyll-a enhancement in the continental shelf southeast of Hainan Island, *J. Mar. Syst.*, *129*, 405–414.